Available online at www.sciencedirect.com
ScienceDirect
Ceramics International 34 (2008) 1797–1803
CERAMICS INTERNATIONAL
www.elsevier.com/locate/ceramint

Microstructure and mechanical properties of yttria-stabilized ZrO_2/Al_2O_3 nanocomposite ceramics

Yinping Ye [a,b,*], Jiangong Li [b], Huidi Zhou [a], Jianmin Chen [a]

[a] State Key Laboratory of Solid Lubrication, Lanzhou Institute of Chemical Physics, Chinese Academy of Sciences, Lanzhou 730000, China
[b] Institute of Materials Science and Engineering, Lanzhou University, Lanzhou 730000, China

Received 1 February 2007; received in revised form 21 March 2007; accepted 12 June 2007
Available online 10 August 2007

Abstract

Yttria-stabilized ZrO_2/Al_2O_3 (abridged as YSZ/Al_2O_3) nanocomposite ceramics were prepared by pressureless sintering of the green sheets of the YSZ/Al_2O_3 nanopowders synthesized by co-precipitation method. The relative density, average grain size, and phase microstructure of the YSZ/Al_2O_3 nanoceramics as a function of YSZ contents were investigated. The relative densities of the YSZ/Al_2O_3 nanoceramics are over 95% as the YSZ contents of the YSZ/Al_2O_3 nanopowders are within 20–85 mol %. The average grain sizes of the ZrO_2 and Al_2O_3 of the as-sintered YSZ/Al_2O_3 nanoceramics decrease with increasing YSZ content of the co-precipitated YSZ/Al_2O_3 nanopowders, while the content of monoclinic ZrO_2 of YSZ/Al_2O_3 nanoceramics increases with increasing YSZ content. The presence of the second phase effectively limits a rapid grain growth of the matrix alumina. The YSZ/Al_2O_3 nanoceramics with an average grain sizes below 80 nm, relative density over 95%, and hardness as high as 19.8 GPa were obtained by the pressureless sintering.

Keywords: A. Sintering; B. Grain size; B. Composites; C. Hardness

1. Introduction

Oxide ceramic materials win wide use in modern technological processes due to a unique combination of physicochemical properties (hardness, refractory characteristics, resistance to aggressive media, etc.). The only shortcoming of the materials, especially in comparison with metals, is the brittlement, which puts substantial limitations to the field of its application and complicates manufacturing of advanced materials. The nanoceramics with nanometer-sized grains provides a possibility for overcoming this disadvantage [1,2]. Superplasticity has been observed in some nanoceramics [3–5], such as the Y_2O_3-stabilized tetragonal ZrO_2 nanoceramics, and the superplastic deformation behavior of the nanoceramics is mainly dependent on small grain sizes [4,6]. Unfortunately, in the pressureless sintering, both processes of the densification and grain growth are driven by diffusion. It is difficult to realize densification without promoting grain growth. Therefore, it is necessary to study the processes of densification versus grain growth in more detail so as to find some clues to resolve this dilemma.

Usually, ceramic desification consists of three stages [7]. The most ceramic densification occurs in the second sintering stage, but a rapid grain growth occurs in the final sintering stage. There is a strong correlation between the onset of a rapid grain growth and the point of 90% relative density. Interestingly, the 90% relative density is the point at which ceramics typically make the transition from the second stage sintering (open pores) to the third stage sintering (closed pores) in the pressureless sintering process [7]. The densification of ceramics is achieved by the shrinkage of the open pores and the grain-boundary diffusion, whereas the dispersed open pores can pin the grain boundary and hinder grain boundary motion, which would in turn suppress the grain growth effectively [8]. A rapid grain growth could occur before the closed pores in the ceramics disappear in the final stage of sintering. There is a degree of resemblance between the presence of the second phase and the open pores pinning the grain boundary, the presence of the second phase may also pin the grain boundary

* Corresponding author at: State Key Laboratory of Solid Lubrication, Lanzhou Institute of Chemical Physics, Chinese Academy of Sciences, Lanzhou 730000, China. Tel.: +86 931 4968150; fax: +86 931 8277088.
E-mail address: yeyinping585@sina.com (Y. Ye).

0272-8842/$34.00 © 2007 Published by Elsevier Ltd and Techna Group S.r.l.
doi:10.1016/j.ceramint.2007.06.005

and hinder grain boundary motion, which would in turn suppress the grain growth effectively [9,10]. However, on this aspect, the preparation of YSZ/Al_2O_3 nanoceramics from the starting powders of alumina particles at submicroscale level and zirconia particle at nanoscale level has been largely focused on, with the zirconia as the second phase [11–14]. These results showed that the second phase limited the matrix Al_2O_3 grain rapid growth; however, the matrix Al_2O_3 grain size still remained at submicroscale level. In order to obtain YSZ/Al_2O_3 nanoceramics with grain sizes of Al_2O_3 and ZrO_2 at nanoscale level, many methods such as co-precipitation method, sol–gel technique and so on have been employed to prepare the starting YSZ/Al_2O_3 nanopowders. For instance, the Al_2O_3/YSZ nanoceramics with high density and an average grain size of about 300 nm was obtained by sintering the green sheets of the 20 wt.% Al_2O_3 doped YSZ powders synthesized by co-precipitation method [15]. Viswanath et al. synthesized the 15 wt.% Al_2O_3 doped YSZ powders by sol–gel technique and obtained the YSZ/Al_2O_3 nanoceramics with full densification and average grain size of less than 60 nm at 1300 °C [16]. The YSZ doped Al_2O_3 matrix nanocomposites have stimulated much research interest because of its low density, high strength, high hardness, and high-temperature stability, but it is hard to obtain Al_2O_3 matrix nanocomposite ceramics with high density and grain size of the matrix at nanoscale level. However, few systematic papers have been reported on the YSZ doped alumina matrix nanocomposite ceramics with grain sizes of Al_2O_3 and ZrO_2 at nanoscale level so far.

In our present work, the yttria-stabilized ZrO_2/Al_2O_3 nanoceramics were fabricated by the pressureless sintering of the green sheets of the YSZ/Al_2O_3 nanopowders containing different YSZ contents synthesized by co-precipitation method. The influences of the YSZ content of the co-precipitated YSZ/Al_2O_3 nanopowders on the relative density, average grain size, phase microstructure, and Vickers microhardness of the YSZ/Al_2O_3 nanoceramics were investigated.

2. Experimental procedure

2.1. Methods

The yttria-stabilized ZrO_2/Al_2O_3 nanocomposite powders were synthesized by a co-precipitation method. Thus the precursor solution of $ZrOCl_2{\cdot}8H_2O$, $Y(NO_3)_3{\cdot}6H_2O$ (corresponding to a composition of 97 mol % ZrO_2 and 3 mol % Y_2O_3) and $Al(NO_3)_3{\cdot}9H_2O$ was prepared by mixing of the three crystals in distilled water. The precursor solution was then mixed with proper amount of 25% ammonia solution to allow the generation of the YSZ/Al_2O_3 precipitates, with the pH value being remained at 9. At the end of the reaction, the precipitates were collected by filtration and washed with distilled water for five times to remove Cl^-, followed by washing with ethanol for three times to remove the residue water. The precipitates were then sequentially dried at 120 °C for 24 h in air, milled in air, and calcinated at predetermined temperature for 2 h, to allow the production of the starting YSZ/Al_2O_3 powders as the raw materials.

The green sheet pellets (15 mm in diameter, 1–2 mm in thickness) were made by uniaxial pressing of the co-precipitated YSZ/Al_2O_3 powders calcinated at 1000 °C at 920 MPa for 5 min in air at room temperature. The YSZ/Al_2O_3 nanoceramics were prepared by heating the green sheets in air at a rate of 10 °C/min up to 1450 °C and sintering for 15 h at the temperature.

2.2. Characterization techniques

X-ray diffraction analysis of the crystalline phases of the calcinated YSZ/Al_2O_3 nanopowders and bulk nanoceramics was performed on a Rigaku D/max-2400 X-ray diffractometer. The mean particle size of the calcinated YSZ/Al_2O_3 powders and average grain size of the bulk nanoceramics were estimated using the Scherrer equation from the diffraction peak widths with the instrument and wavelength related broadening eliminated [17]. Transmission electron microscopy (JEM-1200EX, TEM) was employed to observe the morphology and determine the average grain size of the bulk nanoceramics. The densities of the as-sintered YSZ/Al_2O_3 nanoceramics were measured by the Archimedes method. The relative density was calculated with respect to the theoretical density of tetragonal ZrO_2 (6.10 g cm^{-3}), monoclinic ZrO_2 (5.56 g cm^{-3}) and alpha Al_2O_3 (3.96 g cm^{-3}) [18]. The fraction of monoclinic ZrO_2 in the sintered YSZ/Al_2O_3 nanoceramics was estimated by polymorph method [19].

3. Results and discussion

3.1. Nanopowders

The XRD patterns of the YSZ/Al_2O_3 nanopowders containing different YSZ contents calcinated at 1000 °C are shown in Fig. 1. X-ray diffraction analysis indicates that θ-Al_2O_3, and

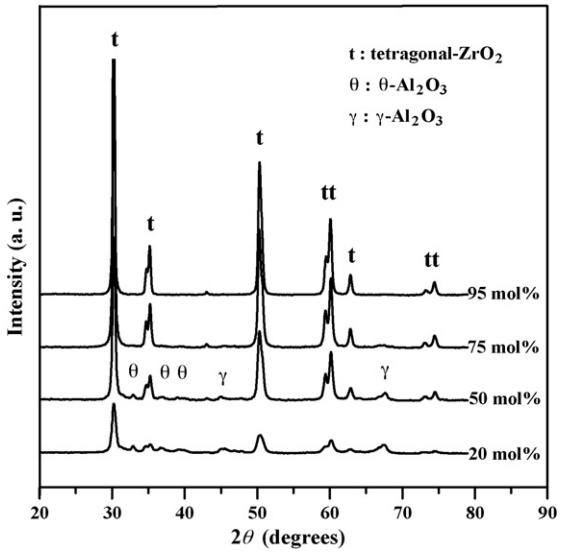

Fig. 1. XRD patterns of the YSZ/Al_2O_3 nanopowders containing different YSZ content calcinated at 1000 °C.

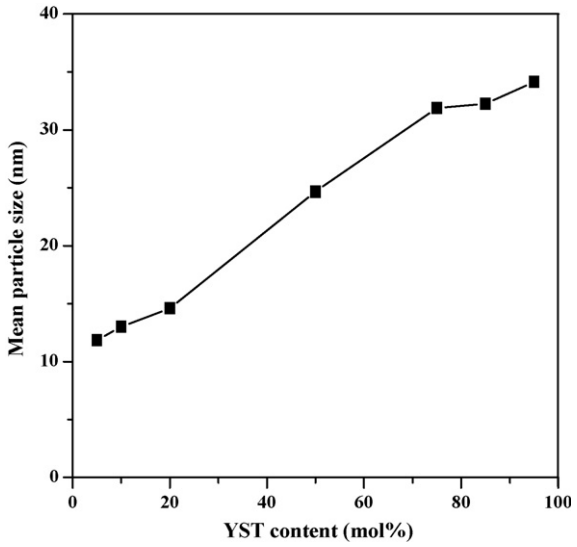

Fig. 2. Mean particle size of the ZrO_2 of the YSZ/Al_2O_3 nanopowders calcinated at 1000 °C as a function of YSZ content.

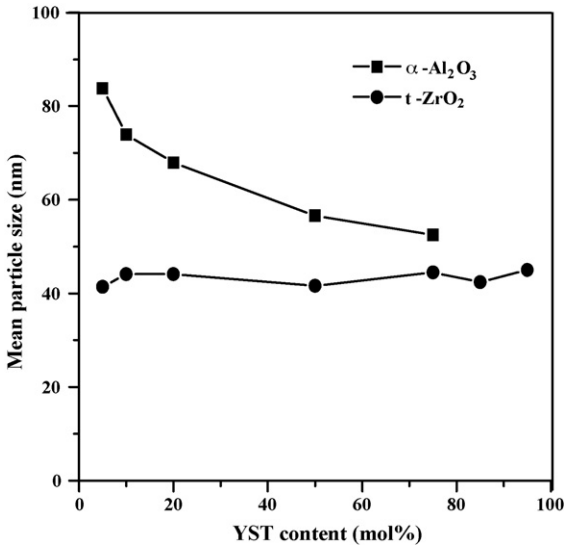

Fig. 4. Mean particle size of the ZrO_2 and Al_2O_3 in the YSZ/Al_2O_3 nanopowders calcinated at 1300 °C as a function of YSZ content.

tetragonal ZrO_2 form by the crystallization of the YSZ/Al_2O_3 powders containing 5–50 mol % YSZ calcinated at 1000 °C and the mean particle sizes of the θ-Al_2O_3 estimated by the Scherrer formula is about 15 nm, whereas the relative intensities of the θ-Al_2O_3 decrease with increasing YSZ content, and only tetragonal ZrO_2 exists as the YSZ content of the YSZ/Al_2O_3 powders is over 75 mol %. This can be attributed to the ability of zirconia to decrease the growth of alumina grains rendering them imperceivable to the X-rays [15,16]. The mean particle size of tetragonal ZrO_2 of the YSZ/Al_2O_3 nanopowders calcinated at 1000 °C calculated by the Scherrer formula is given in Fig. 2. The mean particle size of tetragonal ZrO_2 increases from 12 to 35 nm with increasing YSZ content from 5 to 95 mol %. On calcinations at 1300 °C for 2 h, the zirconia and alumina become fully crystalline and

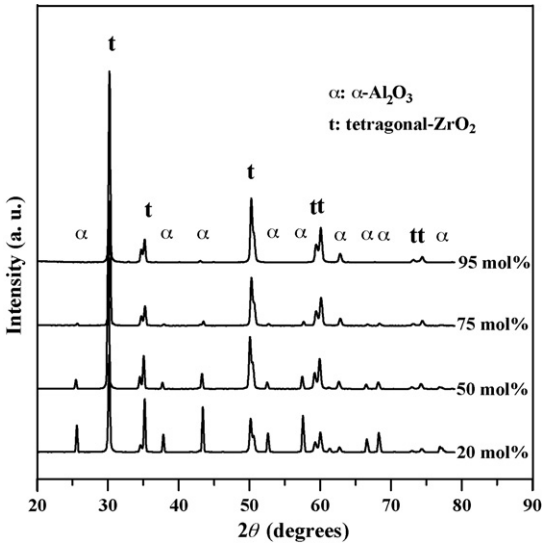

Fig. 3. XRD patterns of the YSZ/Al_2O_3 nanopowders containing different YSZ content calcinated at 1300 °C.

the YSZ/Al_2O_3 nanopowders are composed of α-Al_2O_3 and tetragonal ZrO_2, whereas peaks of monoclinic ZrO_2 do not appear (Fig. 3), which indicates that Al_2O_3 has a stabilizing effect to the tetragonal phase. The mean particle size of the YSZ/Al_2O_3 powders estimated by the Scherrer formula is given in Fig. 4. The mean particle size of Al_2O_3 decreases with increasing YSZ content of the YSZ/Al_2O_3 nanopowders, while the mean particle size of ZrO_2 is within 41–47 nm and keeps almost unchanged with increasing YSZ content. Besides, the mean particle of Al_2O_3 is larger than that of ZrO_2 for all the calcinated YSZ/Al_2O_3 nanopowders, and the mean particle sizes of the Al_2O_3 and ZrO_2 of the YSZ/Al_2O_3 nanopowders are less than 60 nm as the YSZ content exceeds 50 mol %.

It is seen from above the results that the presence of the second phase can elevate the transformation temperature to form α-Al_2O_3 and suppress the mean particle size of α-Al_2O_3 in YSZ/Al_2O_3 nanopowders, which extends the temperature range of slow grain growth of α-Al_2O_3 and provides a possibility to sinter dense nanoceramics without promoting rapid grain growth.

3.2. Sintering and microstructure

In the process of the pressureless sintering of the YSZ/Al_2O_3 nanoceramics, the relative density, average grain size, and phase microstructure of the as-sintered nanoceramics is mostly affected by the YSZ content of the starting YSZ/Al_2O_3 nanopowder. The relative density of the YSZ/Al_2O_3 nanoceramics is over 95% and keeps almost unchanged with increasing YSZ content within 20–85 mol %; whereas it decreases at a too higher (>85 mol %) or too smaller (<20 mol %) YSZ content of the YSZ/Al_2O_3 powders (Fig. 5), which indicates that an improper YSZ content of the YSZ/Al_2O_3 powders is harmful to the densification of the YSZ/Al_2O_3 nanoceramics. The average grain sizes of Al_2O_3 and ZrO_2 of the as-sintered YSZ/Al_2O_3 nanoceramics

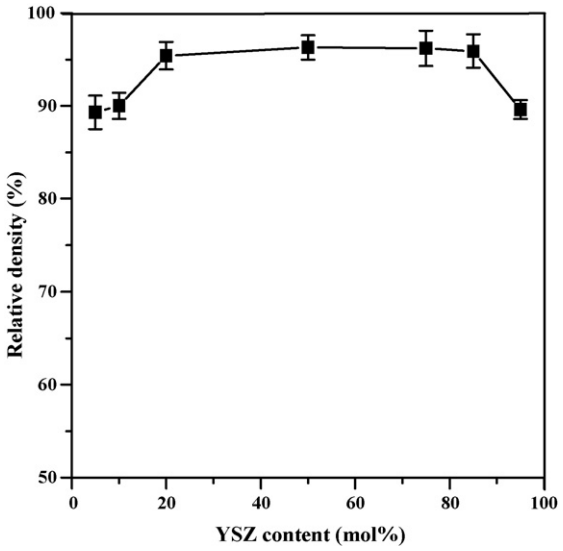

Fig. 5. Relative density of the YSZ/Al_2O_3 nanoceramics as a function of YSZ content.

estimated by the corresponding XRD analysis is shown in Fig. 6. The average grain sizes of Al_2O_3 and ZrO_2 decrease with increasing YSZ content at different paces, depending on the YSZ content. Namely, the average grain size decreases rapidly with increasing YSZ content within 5–20 mol % but it slows at the YSZ content over 20 mol %. Besides, the average grain size of Al_2O_3 is larger than that of ZrO_2 with increasing YSZ content, which is in good agreement with that of the mean particle sizes of the Al_2O_3 and ZrO_2 of the YSZ/Al_2O_3 nanopowders calcinated at 1300 °C with YSZ content (Fig. 4). Fig. 7 shows TEM micrographs of the as-sintered YSZ/Al_2O_3 ceramics from the YSZ/Al_2O_3 nanopowders containing 50 mol % YSZ. The microstructures of the as-sintered YSZ/Al_2O_3 ceramics are typical of ceramics in the final stage of sintering and show no residual porosity. At the same time, some uniaxial grains with clear grain boundaries and polyhedral morphology are also found in the TEM micrographs. The inter- and intra-granular grains of Al_2O_3 and ZrO_2 are quite uniformly distributed and connected in the YSZ/Al_2O_3 nanoceramics (Fig. 7b). The grains of Al_2O_3 (white grins) are larger than the grains of ZrO_2 (black grains). The average grain size of the as-sintered ceramics determined from the TEM observations is about 200–400 nm which is 3–5 times larger than that determined from the corresponding X-ray peak broadening. This is mostly attributed to the microstructure of the inter- and intra-granular grains of Al_2O_3 and ZrO_2 in the YSZ/Al_2O_3 nanoceramics. The grains in the TEM photograph can be agglomerates comprised of several individual grains. The inter- and intra-granular microstructure of the YSZ/Al_2O_3 nanoceramics would induce the formation of the dislocation net or sub-grain-boundary in matrix grains due to the hot stress in the cooling process of the YSZ/Al_2O_3 nanoceramics from a high temperature, and the matrix grains can be broken down into multiple ''sub-grain'' (Fig. 7c), which is in good agreement with what has been reported by Hahn et al. [20] and Kumar et al. [21]. Hahn et al. and Kumar et al. thought that the grains in the TEM photograph could be agglomerates comprised of several individual grains. It is seen from above the results that the presence of the second phase encourages the densification of the as-sintered nanoceramics and limits a rapid grain growth of the matrix alumina in the pressureless sintering. XRD analysis from the corresponding XRD patterns of the as-sintered YSZ/Al_2O_3 nanoceramics (Fig. 8) indicates that a great quantity of monoclinic ZrO_2 forms in the YSZ/Al_2O_3 nanoceramics and the content of the monoclinic ZrO_2 increases with increasing YSZ content. However, no monoclinic ZrO_2 is detected by XRD analysis of the YSZ/Al_2O_3 nanopowders calcinated at 1300 °C (Fig. 3). This can be owe to the crystalline grains obtained more energy and hence became more liable to transform from metastable tetragonal phase to monoclinic phase at increased sintering temperatures [3].

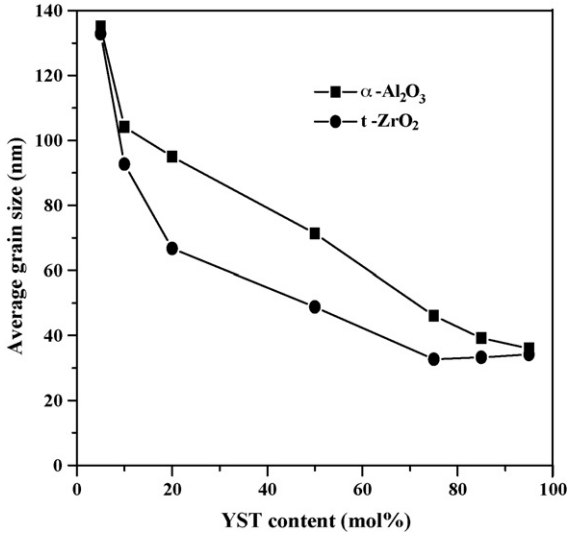

Fig. 6. Average grain sizes of Al_2O_3 and ZrO_2 of the sintered YSZ/Al_2O_3 nanoceramics as a function of YSZ contents.

3.3. Relationship between microstructure and mechanical properties

The variation of the Vickers microhardness of the as-sintered YSZ/Al_2O_3 samples (determined at a load of 2.94 N for 5 s) with YSZ content is shown in Fig. 9. The Vickers microhardness increases with increasing YSZ content up to 20 mol % whereas it assumes a decrease with further increasing YSZ content over 20 mol %. Interestingly, the YSZ/Al_2O_3 nanoceramic sample sintered from the nanopowders containing 20 mol % YSZ has a Vickers microhardness as high as 19.8 GPa, and those sintered from the YSZ/Al_2O_3 nanopowders containing 20–85 mol % YSZ have Vickers microhardness over 16.0 GPa. Usually, the Vickers microhardness of the YSZ/Al_2O_3 ceramics is 12–14 GPa [22,23], whereas the YSZ/Al_2O_3 nanoceramics have a higher microhardness in our present work. This is mostly attributed to the nanostructure of the YSZ/Al_2O_3 nanocomposite ceramics. One of reason of the YSZ/Al_2O_3 nanocomposite ceramics with a higher microhardness is the presence of fine grains and a great quantity of grain-boundary. Firstly, the presence of the second phase ZrO_2 can pin the grain boundary and hinder grain boundary motion, which would in

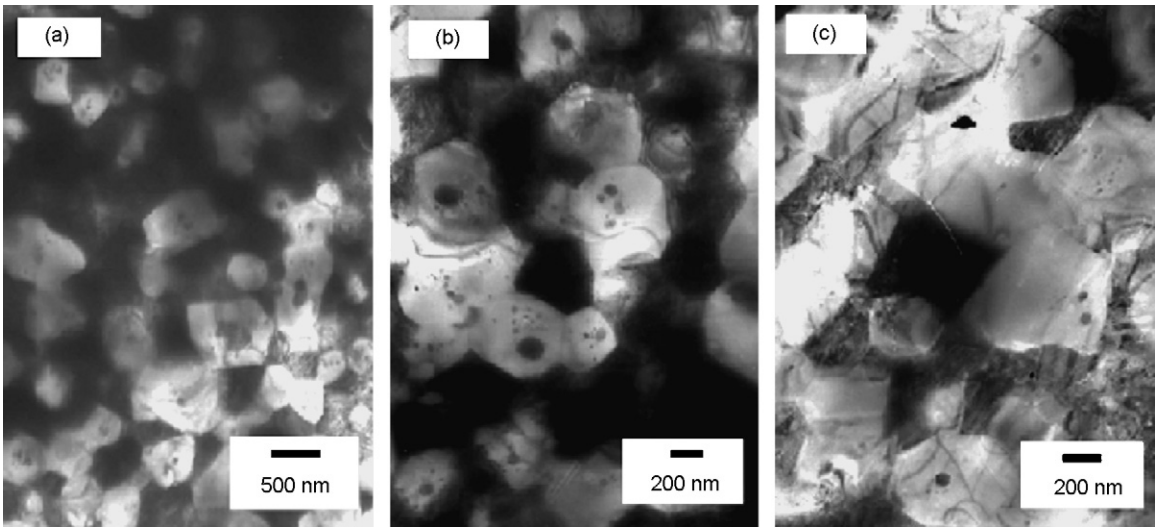

Fig. 7. TEM micrographs of (a) the YSZ/Al_2O_3 nanoceramics from the YSZ/Al_2O_3 nanopowders containing 50 mol % YSZ, (b) and (c) of the magnified images.

turn suppress the grain growth effectively. Secondly, in nanocomposite ceramics, especially in the ZrO_2 matrix nanocomposite ceramics, the dislocation net or sub-grain-boundary forms in matrix grains due to the hot stress in the cooling process of the Y-TZP nanoceramics from a high temperature [24], which results in a decrease of the matrix grain. It is seen from the magnified TEM micrographs of the as-sintered YSZ/Al_2O_3 nanoceramics (Fig. 7c) that the matrix grains is break down into multiple ''sub-grain'' due to the presence of the dislocation net. The fine grains will result in an increase of the microhardness of the YSZ/Al_2O_3 nanoceramics according to Hall-Pech formula. Another reason of the YSZ/Al_2O_3 nanocomposite ceramics with a higher microhardness can be the microstructure of intra-granular grains of Al_2O_3 and ZrO_2 in the YSZ/Al_2O_3 composite ceramics [25]. Because the nanocrystalline grains on the matrix grain and the matrix grain form easily the combining interface of great intensity in the microstructure of intra-granular grains of the YSZ/Al_2O_3 nanocomposite ceramics. These are in favor of an increase of the microhardness of the YSZ/Al_2O_3 nanocomposite ceramics.

In addition, no cracks were found in the indented scars of all the as-sintered samples subject to hardness testing. In order to attest further to the result, the load of the hardness testing was increased from 2.94 N to 9.8 N, no cracks were also found in the indented scars of the as-sintered samples subject to hardness testing (Fig. 10), and the plastic deformation behavior were found in the indented scar edges, which indicate that the as-sintered YSZ/Al_2O_3 nanoceramics have a better fracture toughness than the YSZ/Al_2O_3 ceramics with grain at microscale level because the micrometer-grained YSZ/Al_2O_3 ceramics usually have the formation of cracks in the indented scar edges [26]. Chen et al. thinks that the intragranular dislocation creep is playing an important role in deformation of the YSZ/Al_2O_3 nanocomposite ceramics [27].

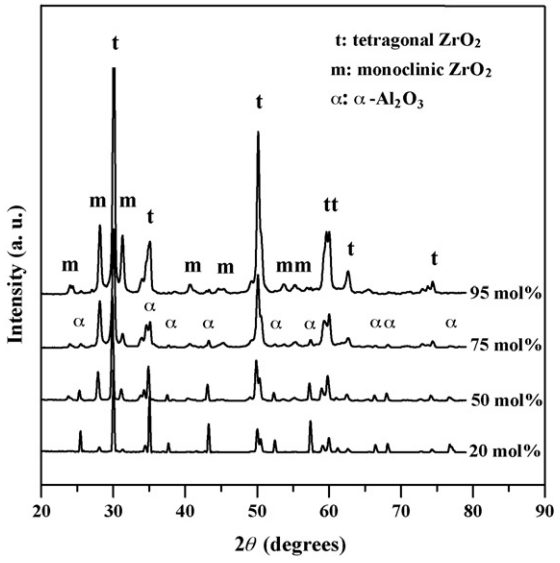

Fig. 8. XRD patterns of the YSZ/Al_2O_3 nanoceramics from the YSZ/Al_2O_3 nanopowders containing various ZrO_2 contents.

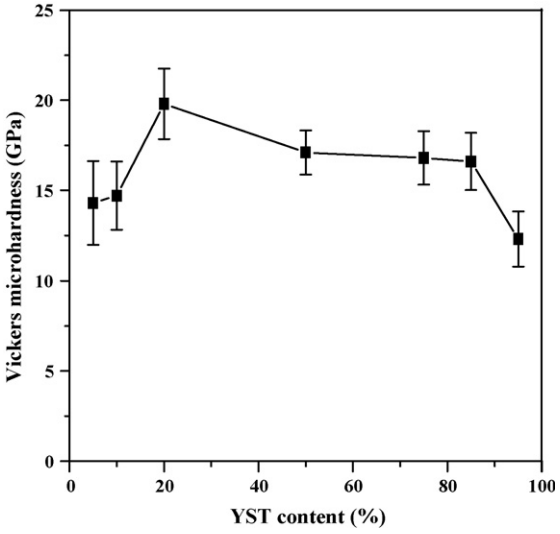

Fig. 9. Relationship between the Vickers microhardness of the YSZ/Al_2O_3 nanoceramics and YSZ content.

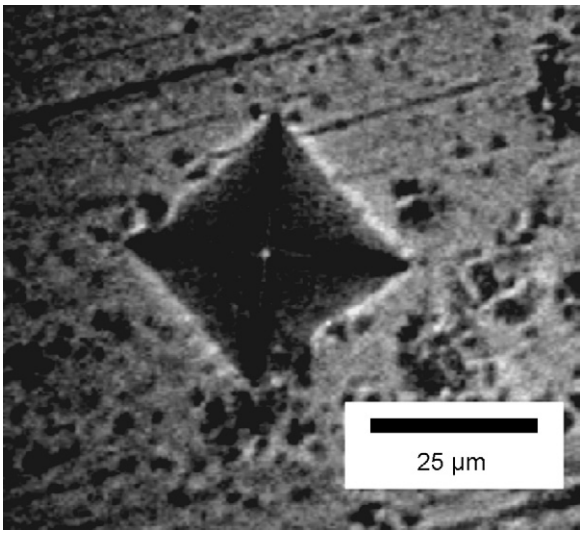

Fig. 10. The indented scar morphologies of the YSZ/Al_2O_3 nanoceramics from the YSZ/Al_2O_3 nanopowders containing 50 mol %ZrO_2 at a load of 9.8 N.

To summarize, the sintering characteristics and microstructures of the YSZ/Al_2O_3 nanoceramics are greatly dependent on the YSZ content of the co-precipitated YSZ/Al_2O_3 powders. In practice, it will be feasible to obtain the YSZ/Al_2O_3 nanoceramics with desirable microstructures and properties by the pressureless sintering of the green sheets of the calcinated YSZ/Al_2O_3 nanopowders with an appropriate YSZ content at relatively low temperature and the as-prepared YSZ/Al_2O_3 nanoceramics with grain at nanoscale level have a better fracture toughness than those with grain at microscale scale level.

4. Conclusions

The co-precipitated YSZ/Al_2O_3 nanopowders calcinated at 1300 °C are composed of α-Al_2O_3 and tetragonal ZrO_2 phases. The mean particle sizes of the Al_2O_3 of the calcinated nanopowders decrease with increasing YSZ content and the mean particle size of Al_2O_3 is larger than that of ZrO_2 for all the calcinated YSZ/Al_2O_3 powders. The sintering characteristics and microstructures of the YSZ/Al_2O_3 nanoceramics are largely dependent on the YSZ content of the co-precipitated YSZ/Al_2O_3 nanopowders. The relative density of the sintered YSZ/Al_2O_3 nanoceramics is over 95% as the YSZ content of the YSZ/Al_2O_3 nanopowders is within 20–85 mol %, whereas the average grain sizes of Al_2O_3 and ZrO_2 decrease with increasing YSZ content. The presence of the second phase limits the matrix alumina rapid grain growth. The Vickers microhardness of the as-sintered YSZ/Al_2O_3 nanoceramics from the YSZ/Al_2O_3 nanopowders containing 20–85 mol % YSZ exceeds 16.0 GPa, whereas The YSZ/Al_2O_3 nanoceramics from the YSZ/Al_2O_3 nanopowders containing 20 mol % YSZ has a Vickers microhardness as high as 19.8 GPa. In addition, no cracks are found in the indented scars of all the as-sintered samples subject to hardness testing, which indicate that the as-sintered YSZ/Al_2O_3 nanoceramics have a better fracture toughness than the micrometer-grained YSZ/Al_2O_3 ceramics.

Acknowledgments

The authors sincerely thank Prof. T. Xu for performance of the TEM observations, Mr. D. Song for XRD, and Dr. P. La and Dr. L. Yu for helpful discussions. This work was supported in part by the Teaching and Research Award Program for Outstanding Young Professors in Higher Education Institute (TRAPOYP), MOE, the Key Research Programs of the MOE, PRC, and the National Natural Science Foundation of China (NSFC) (50272025), and the Innovative Group Foundation from NSFC (50421502).

References

[1] M.J. Mayo, Processing of nanocrystalline ceramics from ultrafine particles, Int. Mater. Rev. 41 (3) (1996) 85–115.
[2] I.W. Chen, L.A. Xue, Development of superplastic structure ceramics, J. Am. Ceram. Soc. 73 (9) (1990) 2585–2609.
[3] J. Karch, R. Brringer, H. Gleiter, Ceramics ductile at low temperature, Nature 330 (6148) (1987) 556–558.
[4] M.J. Mayo, Synthesis and applications of nanocrystalline ceramics, Mater. Des. 14 (6) (1993) 323–329.
[5] F. Wakai, Y. Kodama, S. Sakaguchi, N. Murayama, K. Izaki, K. Niihara, A superplastic covalent crystal composite, Nature 344 (6164) (1990) 421–423.
[6] A. Bravo-Leon, Y. Morikawa, M. Kawahara, M.J. Mayo, Fracture toughness of nanocrystalline tetragonal zirconia with low yttria content, Acta Mater. 50 (18) (2002) 4555–4562.
[7] M.J. Mayo, D.C. Hague, D.J. Chen, Processing nanocrystalline ceramics for applications in superplasticity, Mater. Sci. Eng. A 166 (1–2) (1993) 145–159.
[8] V.V. Srdic, M. Winterer, H. Hahn, Sintering behavior of nanocrystalline zirconia doped with alumina prepared by chemical vapor synthesis, J. Am. Ceram. Soc. 83 (7) (2000) 1853–1860.
[9] U. Betz, A. Sturm, J.F. Loffler, W. Wagner, A. Wiedenmann, H. Hahn, Microstructural development during final-stage sintering of nanostructured zirconia based ceramics, Mater. Sci. Eng. A 281 (1/2) (2000) 68–74.
[10] V.V. Srdic, M. Winterer, G. Miehe, H. Hahn, Different zirconia–alumina nanopowders by modifications of chemical vapor synthesis, Nanostruct. Mater. 12 (1–4) (1999) 95–100.
[11] F.F. Lang, M.M. Hirlinger, Grain growth in two-phase ceramics: Al_2O_3 in ZrO_2, J. Am. Ceram. Soc. 70 (11) (1987) 827–830.
[12] G.J. Liu, H.B. Qiu, R. Todd, R.J. Brook, J.K. Guo, Processing and mechanical behavior Al_2O_3/ZrO_2 nanocomposites, Mater. Res. Bull. 33 (2) (1998) 281–288.
[13] Y. Sakka, T.S. Suzuki, K. Morita, K. Nakano, K. Hiraga, Colloidal processing and superplastic properties of zirconia- and alumina-based nanocomposites, Scripta Mater. 44 (8–9) (2001) 2075–2078.
[14] M. Schehl, L.A. Diaz, R. Torrecillas, Alumina nanocomposites from powder–alkoxide mixtures, Acta Mater. 50 (5) (2002) 1125–1139.
[15] G.B. Prabhu, D.L. Bourell, Synthesis and sintering characteristics of zirconia and zirconia-alumina nanocomposites, Nanostruct. Mater. 6 (1–4) (1995) 361–364.
[16] R.N. Viswanath, S. Ramasamy, Sol–gel derived YSTZ-Al_2O_3 and YSTZ-Al_2O_3-SiO_2 nanocomposites, Nanostruct. Mater. 12 (5–8) (1999) 1085–1088.
[17] K.N.P. Kumar, Growth of rutile crystallites during the initial stage of anatase-to-rutile transformation in pure titania and in titania–alumina nanocomposites, Scripta Metall. Mater. 32 (6) (1995) 873–877.
[18] J.D. Cawley, W.E. Lee, Oxide ceramics, in: R.W. Cahn, P. Haasen, E.J. Kramer (Eds.), Materials Science and Technology, Vol. 11. Structure and Properties of Ceramics, VCH Publishers Inc., New York, NY, USA, 1994 pp. 47–117.
[19] R.C. Garvie, P.S. Nicholson, Phase analysis in zirconia systems, J. Am. Ceram. Soc. 55 (5) (1972) 303–305.

[20] H. Hahn, J. Loga, R.S. Averback, Sintering characteristics of nanocrystalline TiO_2, J. Mater. Res. 5 (3) (1990) 609–614.
[21] K.N.P. Kumar, K. Keizer, A.J. Burggraaf, T. Okubo, H. Nagamoto, S. Morooka, Densification of nanostructured titania assisted by a phase transformation, Nature 358 (6381) (1992) 48–51.
[22] J.S. Hong, L. Gao, S.D.D.L. Torre, H. Miyamoto, K. Miyamoto, Spark plasma sintering and mechanical properties of $ZrO_2(Y_2O_3)$–Al_2O_3 composites, Mater. Lett. 43 (1–2) (2000) 27–31.
[23] B.T. Lee, K.H. Kim, J.K. Han, Microstructures and material properties of fibrous Al_2O_3-(m-ZrO)/t-ZrO_2 composites fabricated by a fibrous monolithic process, J. Mater. Res. 19 (11) (2004) 3234–3241.
[24] M. Sternitzke, Structural ceramic nanocomposites, J. Eur. Ceram. Soc. 17 (9) (1997) 1061–1082.
[25] V.M. Sglavo, P. Pancher, Crack decorating technique for fracture-toughness measurement in alumina, J. Eur. Ceram. Soc. 17 (14) (1997) 1697–1706.
[26] A. Larrea, V.M. Orera, R.I. Merino, J.I. Pena, Microstructure and mechanical properties of Al2O3–YSZ andAl2O3–YAG directionally solidified eutectic plates, J. Eur. Ceram. Soc. 25 (8) (2005) 1419–1429.
[27] G. Chen, K. Zhang, G. Wang, W. Han, The superplastic deep drawing of a fine-grained alumina–zirconiaceramic composite and its cavitation behavior, Ceram. Int. 30 (8) (2004) 2157–2162.